Y. Hos et alii, Frattura ed Integrità Strutturale, 34 (2015) 133-141; DOI: 10.3221/IGF-ESIS.34.14

Focussed on Crack Paths

Measurement and simulation of crack growth rate and direction under non-proportional loadings

Y. Hos
Technische Universität Darmstadt, Materials Mechanics Group, Franziska-Braun-Str. 3, D-64287 Darmstadt, Germany
hos@wm.tu-darmstadt.de

M. Vormwald
Technische Universität Darmstadt, Materials Mechanics Group, Franziska-Braun-Str. 3, D-64287 Darmstadt, Germany
vormwald@wm.tu-darmstadt.de

ABSTRACT. A series of fatigue experiments on thin-walled tubes under tension and torsion, the experimental results – crack path and crack growth life – are measured and compared. It is observed that the cracks follow a curvature from a tensile to a shear dominated growth with increasing crack length. The results are enforced by the high amplitudes applied to the specimens causing large cyclic plastic deformations and crack growth rates in the order of 10^{-3} mm/cycle. The non-linear nature of the cyclic deformation has been taken into account by applying a cyclic plasticity model, and plasticity-induced crack closure is captured by a contact formulation. Already for the uniaxial reference case the current limitations in modelling plasticity induced crack closure – a prerequisite for achieving realistic simulation results – have become obvious. Measurements have shown that friction and roughness induced closure processes come up, especially for non-planar crack surfaces, challenge to be met in the future.

KEYWORDS: Multiaxial fatigue; Mixed mode; Fatigue crack growth.

INTRODUCTION

The fatigue crack growth under non-proportional mixed-mode loading depends on many influence factors besides the mode-mixity. Increasing mode-mixity creates a tendency for a shear dominated crack growth instead of a tensile stress dominated one, the latter being the usual case. With increasing cyclic plastic deformation the shear dominated fatigue crack growth becomes more important. The cyclic plastic deformation is also the origin of the plasticity induced crack closure. Especially in non-proportional cases, the roughness and friction induced crack closure occurs and interacts with the plasticity induced crack closure. These influence factors are closely interrelated, therefore a study of individual factors is hard to achieve.
Originating from information gathered from a literature overview [1], a research project was launched, seeking further knowledge on the mechanisms. Results achieved so far are the subject of this paper. In order to connect the results to the state of the art the experimental methods are first applied to cases with proportional and mode I dominated fatigue crack growth.

DESCRIPTION OF THE PROBLEM

Constant amplitude fatigue tests have been performed using thin-walled tubes under tension-compression (force F) and torsion (moment M). The specimen geometry is shown in Fig. 1. The specimens were machined from longitudinally welded tubes. The individual specimens were saw-cut and the notches were milled. Two holes, diameter 4 mm, were drilled with the distance of 10 mm of the centres of the holes (length of an arc measured at the outer surface). The notch was positioned opposite to the longitudinal weld. The material is the construction steel S235 with mechanical properties as given in Tab. 1. Besides Young's modulus, E, plastic offset stress, $R_{p0.2}$, ultimate tensile strength, R_m, the parameters of the cyclic stress-strain curve,

$$\varepsilon_a = \frac{\sigma_a}{E} + \left(\frac{\sigma_a}{K'}\right)^{\frac{1}{n'}}, \tag{1}$$

are given. For use in finite element calculations the cyclic stress-strain curve is reformulated in terms of Chaboche's model [2],

$$\sigma = \sigma_y + \sum_1^5 \left[\frac{C_i}{\gamma_i}\left(1 - \exp\left(-\gamma_i \varepsilon_{pl}\right)\right)\right], \tag{2}$$

with the parameters listed in Tab. 2.

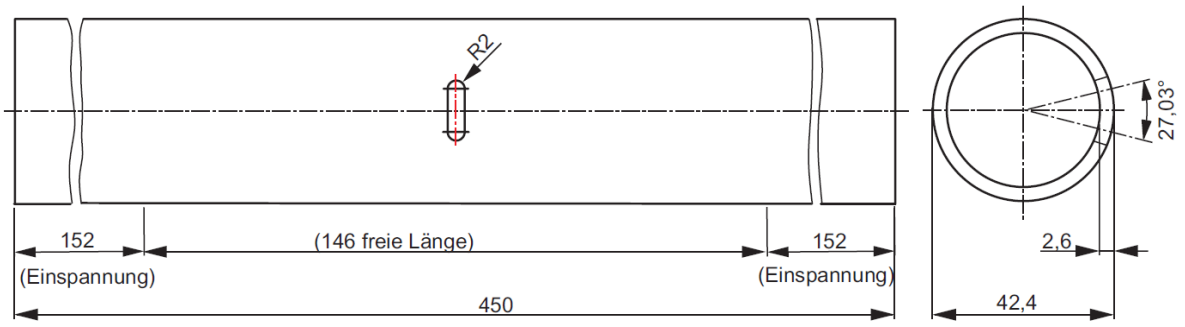

Figure 1: Specimen geometry.

E in MPa	$R_{p0.2}$ in MPa	R_m in MPa	K' in MPa	n'
214000	310	435	1170	0.239

Table 1: Mechanical properties of S235 [3].

σ_y in MPa	C_1 in MPa	γ_1	C_2 in MPa	γ_2	C_3 in MPa	γ_3	C_4 in MPa	γ_4	C_5 in MPa	γ_5
58.2	13442	46	39134	400	72245	1904	603494	7404	800707	104861

Table 2: Chaboche parameters for representing the cyclic stress strain curve of S235.

Two series of experiments have been performed. In the first series of experiments, the fatigue crack lengths were monitored automatically by taking photographs of the specimen at predefined numbers of applied cycles. Three cameras were installed, one directly facing the slit of width 14 mm from front, one with 45° angle on one side and one with 45° angle on the other side. At regular, pre-defined intervals the test was interrupted automatically. The specimen was

unloaded completely. Then, a static load of 90% of the maximum fatigue load was applied. During the short hold time the cameras took pictures of the specimen's surface. The specimen was unloaded again and the cyclic loading continued. The pictures were inspected after the test. In order to ease the optical evaluation of the crack tip coordinates the specimens were branded with a 1 mm Laser-dot pattern prior to testing.

The five different loading sequences have been applied: pure tension-compression loading, pure torsion loading, proportional loading resulting from the superposition of these two and out-of-phase loading with phase angles of 45° and 90°. The load ratio was $R_F = R_M = -1$. The experiments have been conducted under load control and moment control, respectively, using a servo-hydraulic, four-pillar tension-torsion testing machine with frequencies between 0.25 Hz and 2 Hz. In the air conditioned laboratory, a temperature of 21°C and a relative air humidity of 50% were kept constant.

The cracks were assumed to be through-wall cracks with a straight crack front. The crack length is defined as the arc length with the arc starting at the crack initiation location. Here, the scheme of presenting the results was adopted from references [4] an [5] with crack 1 being left and crack 3 being right.

In the second series of experiments the tests were occasionally interrupted and the deformation field was measured applying the digital image correlation (DIC) technique. More details on the measurement technique can be found in references [6,7]. Some results of these investigations are used later when dealing with crack closure.

Uniaxial Loading

The specimen R-001 has been tested under pure tension-compression loading with $F_{max} = 45\,\text{kN}$ and $R_F = -1$. Two symmetric cracks grew in the centre cross section plane, Fig. 2. The crack growth curve is shown in Fig. 3.

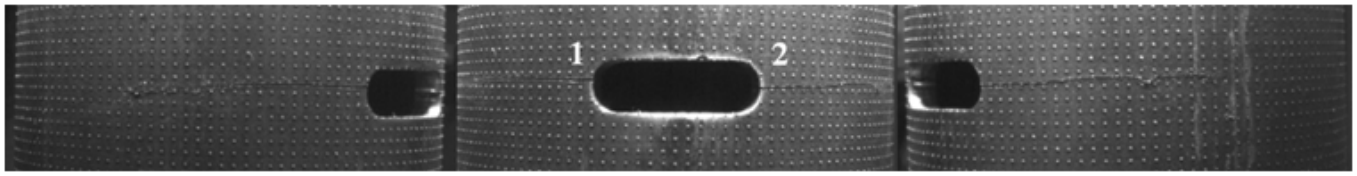

Figure 2: Cracks in the specimen R-001, pure tension-compression with $F_{max} = 45\,\text{kN}$ and $R_F = -1$, steel S235.

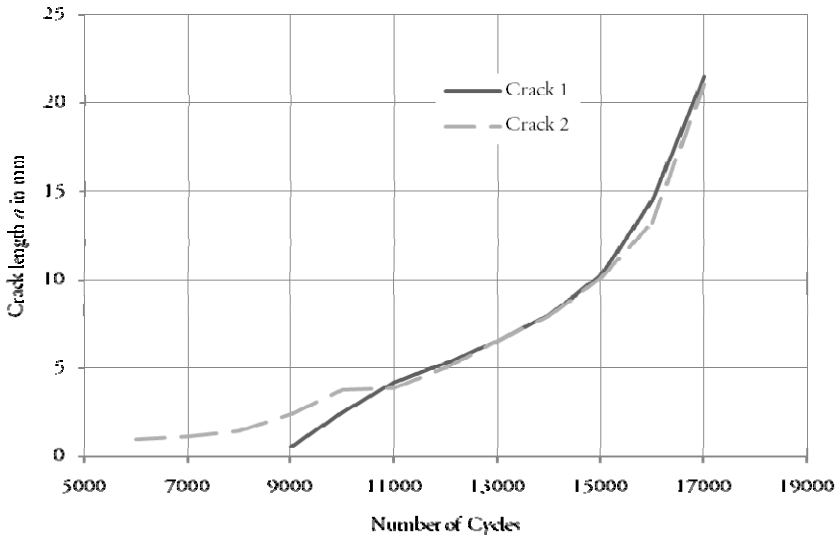

Figure 3: Crack growth curve of specimen R-001, pure tension-compression with $F_{max} = 45\,\text{kN}$ and $R_F = -1$, steel S235.

The results of this experiment serve as a reference for determining the basic material crack growth properties and for calibrating numerical procedures.

Multiaxial Loading

Three specimens were tested under proportional loading, 90° out-of-phase loading and 45° out-of-phase loading, namely the specimens R-004, R-005 and R-006 respectively. The amplitudes of the loadings are $F_{\max} = 33\,\mathrm{kN}$, $M_{\max} = 382\,\mathrm{Nm}$ and $R_F = R_M = -1$. The nominal stresses in the gross section are $\sigma_{n,\max} = 101.5\,\mathrm{MPa}$ and $\tau_{n,\max} = 62.6\,\mathrm{MPa}$. Again, two cracks initiated at the notch. Only for the very early stage of short fatigue crack growth it can be assumed that the crack grows in the uniaxial stress field prevailing at the notch surface. The different crack paths can be seen in Figs. 4 to 6 with a summary in Fig. 7.

For proportional loading, Fig. 4, the principal axis calculated from the nominal stresses is 25.5° inclined against the specimen axis. The crack growth direction, however, is only inclined approximately 14° against the cross section plane. Some cyclic mode II loading could have contributed to the fatigue crack growth. The specimen does not show the conventional and expected growth behaviour under pure mode I.

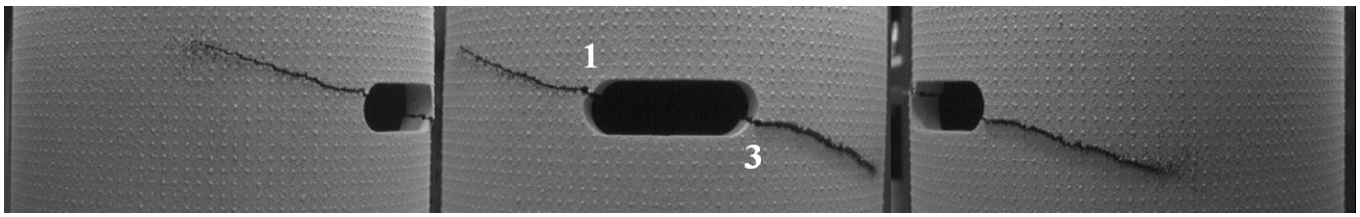

Figure 4: Cracks in specimen R-004, proportional loading with $F_{\max} = 33\,\mathrm{kN}$, $M_{\max} = 382\,\mathrm{Nm}$ and $R_F = R_M = -1$, steel S235.

For out-of-phase loading with phase angle 90° the two cracks show unsymmetrical growth behaviour, Fig. 5. While crack 1 grows straight at nearly 45° inclined to the specimen axis, crack 3 starts curving almost immediately after initiation. The crack has at least two options for choice which path to follow and both options are nearly equilibrate. The crack growth life – the comparison is shown in Fig. 8 – under the 90° out-of-phase loading is longest.

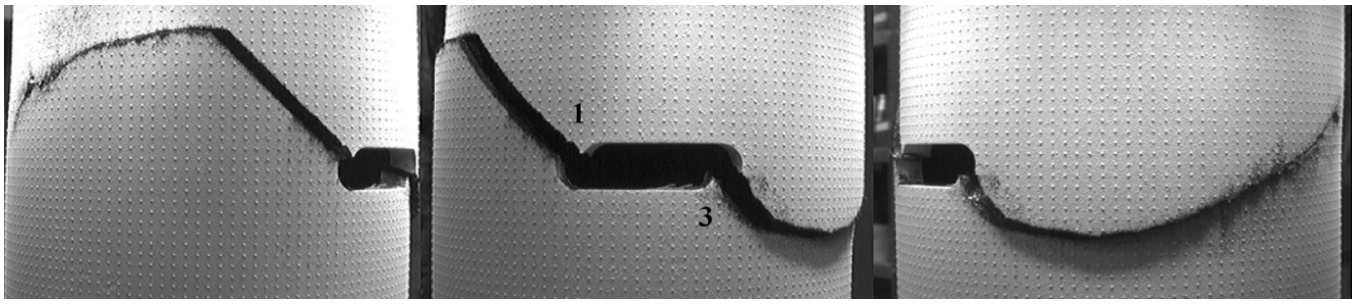

Figure 5: Cracks in specimen R-005, out-of-phase loading with $F_{\max} = 33\,\mathrm{kN}$, $M_{\max} = 382\,\mathrm{Nm}$ and $R_F = R_M = -1$, phase angle 90°, steel S235.

Under out-of-phase loading with phase angle 45° crack 1 is inclined in average 26° during its first 13 mm of growth and afterwards turns to a direction perpendicular to the specimen axis. Contrary to crack 1 the crack 3 shows an initial steep crack path inclined 58° against the cross section plane. After 12 mm of crack growth a sharp kink to the cross section plane growth occurs. The stepwise crack growth, see Fig. 6, is related to the various kinks in the crack growth direction. After the occurrence of a kink the growth rate is decelerated. As a consequence of the variety of kinks the crack surface becomes very rough. In total, the crack growth is slower than under proportional loading which might be due to increased roughness induced crack closure. The frequency of kinks and the unsymmetrical growth of the two cracks may again indicate that the crack path has at least two options for choice which are nearly equilibrate. In its early stage the mode I growth around the notch surface dominates. With increasing crack length a fracture mode II gains priority and is enforced after approximately 13 mm of crack growth.

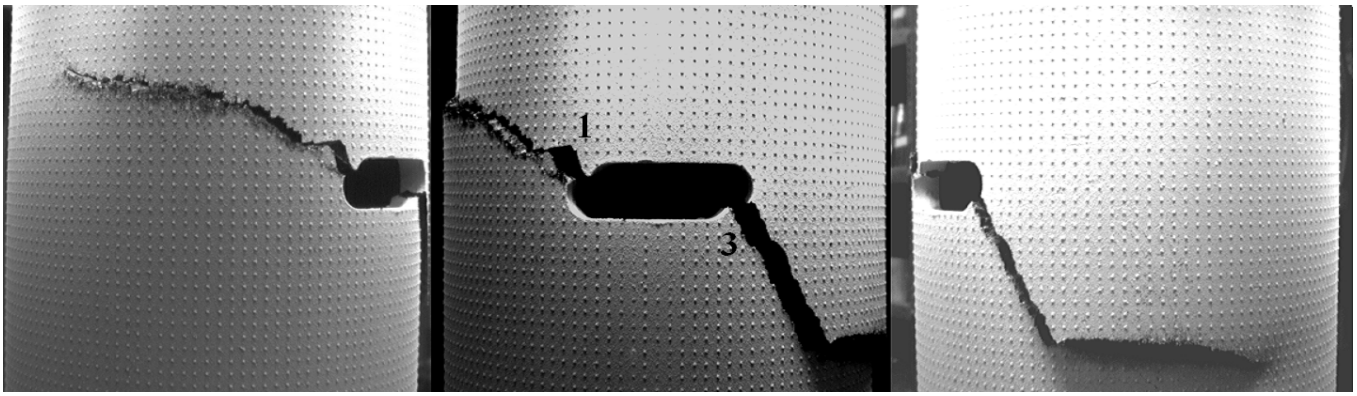

Figure 6: Cracks in specimen R-006, out-of-phase loading with $F_{max} = 33\,\text{kN}$, $M_{max} = 382\,\text{Nm}$ and $R_F = R_M = -1$, phase angle 45°, steel S235.

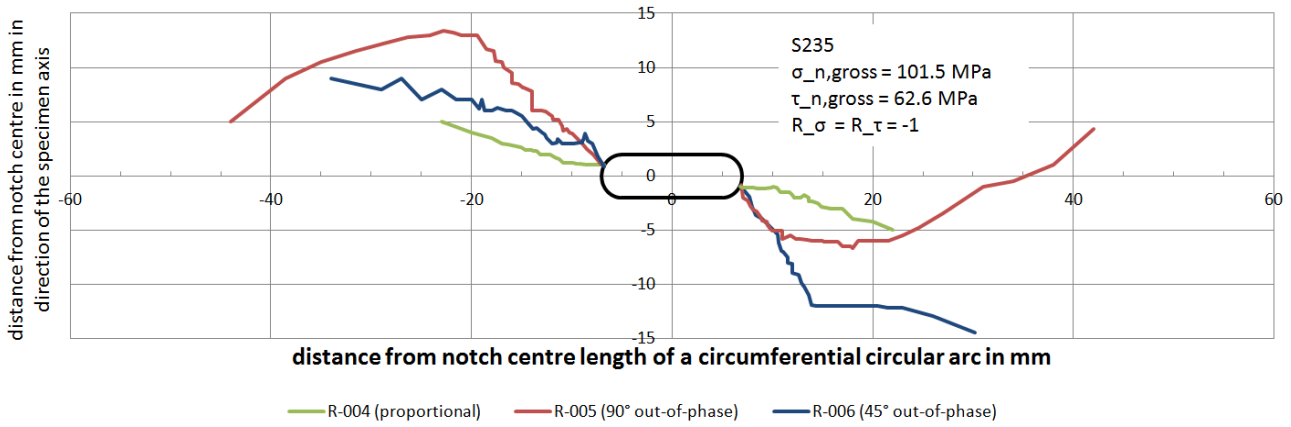

Figure 7: Crack growth curve of specimens R-004, R-005 and R-006 with $F_{max} = 33\,\text{kN}$, $M_{max} = 382\,\text{Nm}$ and $R_F = R_M = -1$, steel S235.

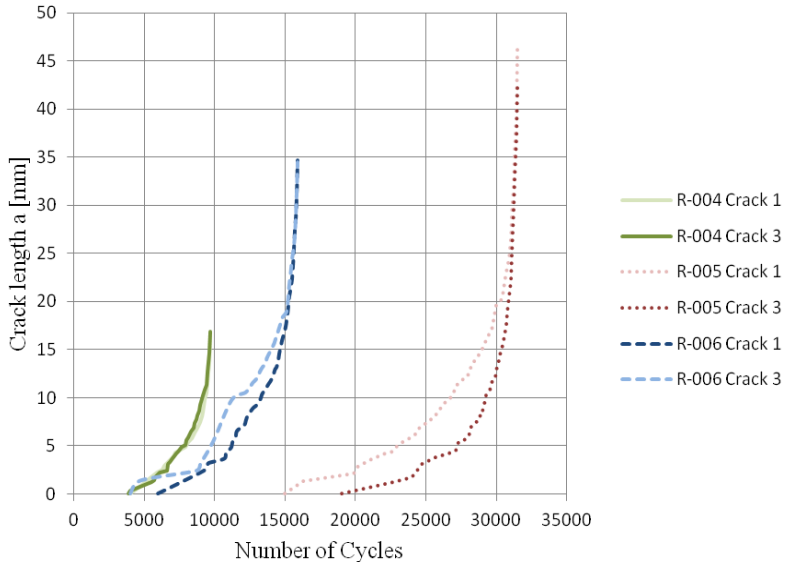

Figure 8: Crack growth curve of specimens R-004, R-005 and R-006 with $F_{max} = 33\,\text{kN}$, $M_{max} = 382\,\text{Nm}$ and $R_F = R_M = -1$, steel S235.

FATIGUE CRACK GROWTH SIMULATION

In the experiments presented in the previous chapter the applied load amplitudes have been so large and the crack growth rates have been so fast that a fatigue crack growth simulation is expected to fail when based on the stress intensity factor range of the linear elastic fracture mechanics. From the variety of crack driving force parameters of the elastic-plastic fracture mechanics [8] the cyclic ΔJ-integral was selected for describing fatigue crack growth,

$$\Delta J = \int_{\Gamma} \left(\Delta W \, \mathrm{d}y - \Delta T_i \frac{\partial(\Delta u_i)}{\partial x} \mathrm{d}s \right) \tag{3}$$

with

$$\Delta W = \int_0^{\Delta \varepsilon_{ij}} \Delta \sigma_{ij} \, \mathrm{d}(\Delta \bar{\varepsilon}_{ij}) \, . \tag{4}$$

The symbol Δ preceding the stress tensor, strain tensor, traction vector and displacement vector components designates the changes of these quantities. These changes must be evaluated referring to a reference state. It serves as the new origin for defining the increments of the field variables, the latter preceded by the symbol Δ. The stress and displacement state at the moment of load reversal is a natural reference state. Then the symbol Δ designates the increments from the respective reference values. At the moment of the next reversal, these increments become the conventional cyclic ranges. However, the symbol Δ in ΔJ and ΔW does not represent changes of J and W; instead ΔJ and ΔW are functions of their arguments as defined by Eqs. (3) and (4).

For non-proportional loading the theoretical background is widely lost. Nevertheless, Hertel et al. [9] proposed an algorithm which delivers practically path-independent values when solving Eq. (3). Due to this path independence the thereby obtained value should be valid crack driving force. In case of non-proportional loading the load reversal points, in terms of ΔJ, are detected by the following algorithm. If the change in ΔJ after the integration of Eq. (3) turns out to be negative, it is presumed that the last equilibrium state was a load reversal point. In consequence, the reference variables are redefined with stress, strain and displacement values of the last equilibrium state. Thereupon, the integration is continued. This procedure provides the monotonic increase of ΔJ for every load step.

Hertel's algorithm was extended here to take crack closure into account. Only the portions of a cycle with open crack surfaces have been considered. Therefore, the values obtained here can be labelled effective cyclic J-integral, ΔJ_{eff}. The loading step associated with the onset of crack closure was determined by applying a finite element based crack growth simulation.

In the present paper only results for the tension-compression can be reported. The simulation started with three cycles applied to the uncracked structure. At maximum load of the next cycle, a crack growth step for 1 mm crack advance was executed. For this purpose the boundary condition of the relevant nodes on the crack growth plane was changed from fixed to unrestrained. Additionally, a contact plane was inserted at the new crack surface to prevent negative displacements of the crack surface nodes during subsequent cyclic loading. After the new equilibrium was found three cycles without crack growth were calculated. The node release procedure – 1 mm crack growth followed by three cycles – was repeated until reaching 5 mm crack length. Further repetitions of this scheme followed until reaching a crack length of 6 mm. However, the crack growth per repetition was continuously reduced. Growth steps of 0.5 mm, 0.25 mm and two times 0.125 mm were used. It is admitted that sound recommendations, see e.g. Herz et al. [10,11] and Zerres and Vormwald [12], for achieving a converged result are violated. However, with the plasticity model at hand converged results cannot be achieved either due to its ratcheting properties. A first estimate is expected to provide inside anyway.

In Fig. 9 an example is shown for the dependence of ΔJ_{eff} from the stress range $\Delta\sigma$. The calculations were stopped on the occurrence of the first crack surface contact. Recently, Hos et al. [6,7] showed that due to severe ratcheting the crack opening displacements increase from cycle to cycle without any trend of stabilization. This behaviour is typical for the Chaboche model. As a consequence of the large ratcheting the crack opening and closure loads are too low when compared to measured values using the digital image correlation technique. In contrast to the simulations presented in [7] the node release scheme was modified to reduce ratcheting. In especially, no intermediate cycles without a crack growth

step were applied. Nevertheless, before dealing with the more complicated combined loading cases producing non-proportional mixed mode a realistic cyclic plasticity model has to be implemented. Such models are available [13]; however, their application requires determination of material's ratcheting behaviour first and identification of the corresponding material parameters second. Such work is ongoing.
The numerical as well as the experimental determination of crack closure is accompanied by some uncertainties which are transferred to the effective ranges of the crack driving force parameter. Fig. 10 is shown here with the intension to unravel the uncertainties. First, an expected crack growth rate as function of the effective cyclic is plotted as solid line. A power law is assumed to correlate both variables.

$$\frac{\mathrm{d}a}{\mathrm{d}n} = C \cdot \Delta J_{\mathrm{eff}}^{m} \tag{5}$$

The parameters C and m are determined following an older recommendation [14] that the exponent might be set to m = 1.5 and the coefficient can be estimated from a fatigue crack growth rate of 10^{-5} mm/cycle at $\Delta J_{\mathrm{eff}} = E/(5{\cdot}10^{5}\ \mathrm{mm}^{-1})$. Second, the experimentally determined crack growth rates of specimen R-001 are plotted as line-connected symbols over ΔJ_{eff} where this effective crack driving force is estimated based on both numerically and experimentally determined effective ranges. It can be concluded that the measured effective ranges provide more realistic estimates of the crack driving force.

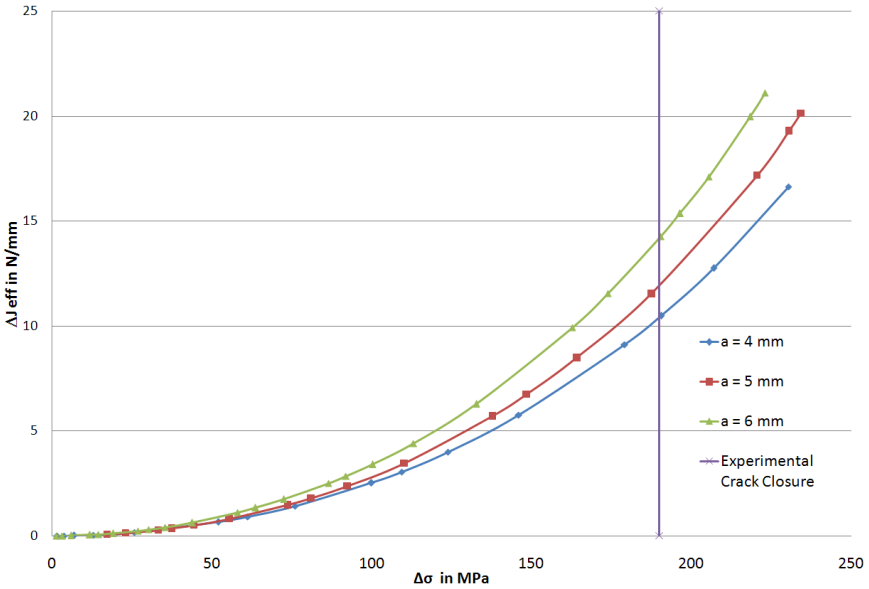

Figure 9: ΔJ_{eff} as function of the applied nominal stress range $\Delta\sigma$, specimen R-001, pure tension-compression with $F_{\max} = 45\,\mathrm{kN}$ and $R_F = -1$, steel S235.

CONCLUSIONS

The path of fatigue cracks in thin walled tubes under combined tension/compression and torsion has been experimentally determined for proportional and non-proportional loading. As a general trend, it is observed that the cracks follow a curvature from a tensile to a shear dominated growth with increasing crack length. This behaviour had been observed also in previous investigations, however, an influence of the specimen geometry explaining the effect had bee postulated because the former specimens were shouldered. Here, it must be stated that the change of the growth mode is a property of the material itself. This change was observed to occur either in a continuous way or abruptly producing a kink. Both phenomena could appear in the same specimen at the both crack tips.
The results summarized above are probably enforced by the high amplitudes applied to the specimens causing large cyclic plastic deformations and crack growth rates in the order of 10^{-3} mm/cycle. Any fracture mechanics based model for

describing the process should therefore be based on a crack driving force parameter of the elastic-plastic fracture mechanics. Here, the closure-free cyclic ΔJ_{eff} is applied first to the uniaxial case. Even for this relatively simple case the problem of realistically estimating the effective ranges becomes apparent. The simulation with a finite element based node release scheme requires the application of an advanced plasticity model which is superior to the Chaboche model as it is supplied in commercial software. Especially ratcheting should be described realistically as this process occurs near the crack tips in a very pronounced way. Otherwise the predicted plasticity induced crack closure is unrealistic.
Without a satisfactory solution for determining the plasticity induced crack closure the non-proportional mixed mode case is hard to tackle. First measurements have shown that – and this is obvious – friction and roughness induced closure processes come up, especially for non-planar crack surfaces. This modelling challenge will have to be met in the future.

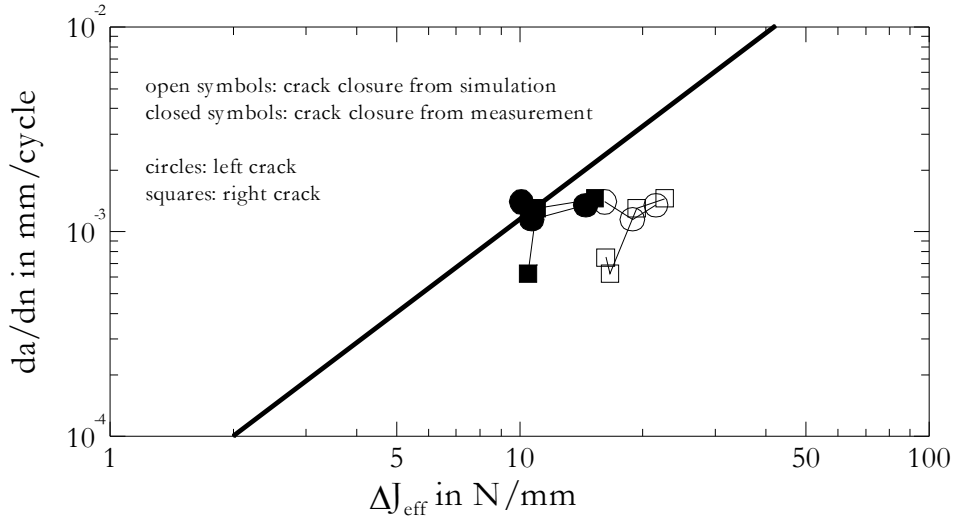

Figure 10: Experimentally determined fatigue crack growth rates from specimen R-001, pure tension-compression with $F_{\max} = 45\,\text{kN}$ and $R_F = -1$, steel S235, plotted over ΔJ_{eff} the latter calculated for measured and simulated effective ranges.

ACKNOWLEDGEMENT

The German Research Foundation (Deutsche Forschungsgemeinschaft) is greatly acknowledged by the authors for financial support under grant Vo729/13-1.

REFERENCES

[1] Zerres, P., Vormwald, M., Review of fatigue crack growth under non-proportional mixed-mode loading, International Journal of Fatigue 58 (2014) 75–83.
[2] Chaboche, J.L., Dang Van, K., Cordier, G., Modelization of the strain memory effect on the cyclic hardening of 316 stainless steel, 5th Int. Conf. Struct. Mech. in Reactor Techn., L (1979) L11/3.
[3] Boller, Chr., Seeger, T., Materials data for cyclic loading, Elsevier, 1 (1987).
[4] Zerres, P., Brüning, J., Vormwald, M., Risswachstumsverhalten der Aluminiumlegierung AlMg4.5Mn unter proportionaler und nichtproportionaler Schwingbelastung, Materials Testing, 53 (2011) 109-117.
[5] Zerres, P., Brüning, J., Vormwald, M., Fatigue crack growth behavior of fine-grained steel S460N under proportional and non-proportional loading, Engineering Fracture Mechanics, 77 (2010) 1822-1834.
[6] Hos, Y., Vormwald, M., Freire, J.L.F., Using digital image correlation to determine mixed mode stress intensity factors in fatigue cracks, Proceedings of COTEQ 2015, Conference on Technology of Equipment, organized by ABENDI, Brazilian Society for NDT and Inspection, (2015).
[7] Hos, Y., Vormwald, M., Freire, J.L.F., Measurement and simulation of strain fields around crack tips under mixed-mode fatigue loading, Frattura ed Integrità Strutturale, 42 (2015) 42-55. DOI: 10.3221/IGF-ESIS.33.06.

[8] Vormwald, M., Fatigue crack propagation under large cyclic plastic strain conditions, Procedia Materials Science, 3 (2014) 301-306.
[9] Hertel, O., Döring, R., Vormwald, M., Cyclic J-integral under nonproportional loading, Proc. 7th Int. Conf. Biaxial/Multiaxial Fatigue Fract., DVM Berlin, (2004) 513-518.
[10] Herz, E., Hertel, O., Vormwald, M., Numerical simulation of plasticity induced fatigue crack opening and closure for autofrettaged intersecting holes, Engineering Fracture Mechanics, 78 (3) (2011) 559-572.
[11] Herz, E., Thumser, R., Bergmann, J.W., Vormwald, M. Endurance limit of autofrettaged Diesel-engine injection tubes with defects, Engineering Fracture Mechanics, 73 (2006) 3-21.
[12] Zerres, P., Vormwald, M., Finite element based simulation of fatigue crack growth with a focus on elastic–plastic material behavior, Computational Materials Science, 57 (2012) 73–79.
[13] Döring, R., Hoffmeyer, J., Seeger, T., Vormwald, M., A Plasticity Model for Calculating Stress-Strain Sequences Under Multiaxial Nonproportional Cyclic Loading, Computational Material Science, 28 (2003) 587-596.
[14] Vormwald, M., Anrißlebensdauervorhersage auf der Basis der Schwingbruchmechanik für kurze Risse, Institut für Stahlbau und Werkstoffmechnaik der Technischen Universität Darmstadt, report 47 (1989).